Robotics and Autonomous Systems 160 (2023) 104310

Contents lists available at ScienceDirect

Robotics and Autonomous Systems

journal homepage: www.elsevier.com/locate/robot

On the parameter identification of free-flying space manipulator systems

Olga-Orsalia Christidi-Loumpasefski [*,1], Evangelos Papadopoulos

School of Mechanical Engineering, National Technical University of Athens, 15780 Athens, Greece

ARTICLE INFO

Article history:
Received 21 August 2020
Received in revised form 11 September 2022
Accepted 5 November 2022
Available online 15 November 2022

Keywords:
Parameter identification
Space manipulator systems
Space robotics
On-orbit servicing

ABSTRACT

A novel parameter identification method is proposed, which identifies all the parameters required for the reconstruction of free-flying space manipulator system dynamics. Its key advantage is that it does not use acceleration measurements; thus, it is less sensitive to sensor noise than other methods. The method is based on the conservation of angular momentum and on a kinematic equation including a Jacobian. To apply the method, all manipulator joints are commanded to follow optimized exciting trajectories, while the system is in free-floating mode. The estimated parameters render the free-flying system dynamics fully identified and available to model-based control. The method applies to multi-arm systems and is validated by simulation and experiments with excellent results.

1. Introduction

Space is becoming fast very important, not only for exploration but also for people's well-being. However, space operations face numerous challenges. Spacecraft failures can disrupt critical services and contribute to the generation of space debris. On Orbit Servicing (OOS) allows for the development and maintenance of vital on orbit infrastructure, including operations such as re-orbiting and de-orbiting, inspection and retrofitting of structures, satellite maintenance and repair, and space debris removal. A number of manned on-orbit servicing missions have been accomplished successfully, while autonomous servicing is planned for the near future.

A cost-effective way to accomplish OOS is to employ Free-Flying Space Manipulator Systems (FFSMS) [1]. FFSMS consist of one or more robotic manipulators, mounted on a spacecraft (SC) equipped with thrusters, reaction wheels (RWs), antennas and sensors, see Fig. 1. The ETS-7 and the Orbital Express are examples of such systems [2,3]. Unlike fixed-based robots, the FFSMS spacecraft is disturbed by manipulator motions, [4]. Hence, to control such a system, it is essential to consider the dynamic coupling between the manipulators and their base. A number of control modes for FFSMS have been proposed and can be classified in three categories [5]. In the first, both the position and attitude of the SC are actively controlled (*free-flying mode*).

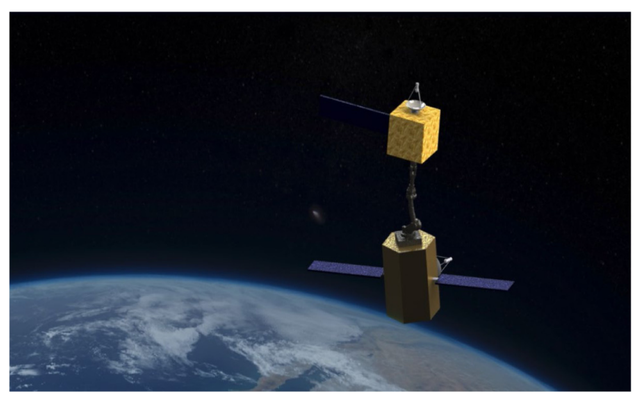

Fig. 1. A free-flying space manipulator system with a captured satellite.

In the second mode, neither is controlled (*free-floating mode*), and finally, in the third, only the SC attitude is controlled. During different phases of a mission, a succession of these modes can be employed.

To accomplish high accuracy tasks on orbit, advanced control strategies such as model-based ones, must be employed. However, model-based control requires accurate knowledge of a system's parameters [6]. Also, these are important for accurate navigation algorithms, for system validation, and for failure detection. In addition, the FFSMS parameters can change on orbit for a number of reasons, such as docking to a spacecraft or space debris capture, and therefore they must be updateable on orbit. The parameters can be obtained approximately through

* Corresponding author.
E-mail addresses: olgachr@central.ntua.gr (O.-O. Christidi-Loumpasefski), egpapado@central.ntua.gr (E. Papadopoulos).

1 Olga-Orsalia Christidi-Loumpasefski was supported by an Onassis Foundation Scholarship, Greece.

https://doi.org/10.1016/j.robot.2022.104310
0921-8890/

detailed system CAD models. Nevertheless, many elements are very complex to model [7]. Therefore, such models can be useful for obtaining initial estimates only.

To address these needs, a number of parameter identification methods have been developed. These methods can be classified as those employing the equations of motion, those based on energy methods, and those based on momentum equations. Examples of the former include [8–12]. However, the main disadvantage of the equations of motion methods is the requirement for acceleration measurements, which contain substantial noise and corrupt the estimates.

Xu et al. [13] proposed a method that uses both equations of motion and momentum equations, for identifying all inertial properties of a space manipulator system and of a grasped target. Hence, the method requires acceleration measurements and many steps to identify system parameters.

To tackle this limitation, other researchers have formulated identification methods based solely on energy or momentum equations, [8,14–18]. However, these algorithms, cannot identify all required parameters; they estimate mainly the SC body or the grasped object. A momentum method for identifying the parameters of a space robot was proposed, that identifies all parameters required to reconstruct the *free-flying* dynamics, using the linear and angular momentum equations [19]. However, during the identification experiment, the method requires the use of reaction wheels, increasing operational complexity, while the regressor matrix of the angular momentum requires the additional measurements of the spacecraft linear velocity, increasing noise sensitivity. Also, it assumes that the system momentum is known and applied by the reaction wheels; however, this is not developed further to include this assumption explicitly. A recent review of system identification methods for space manipulator systems can be found in [20].

In our previous works [21,22], methods for identifying *all* system parameters required for the complete reconstruction of a system's *free-floating* joint space dynamics [21] and Cartesian space dynamics [22] respectively, were proposed. Compared to the ones in the literature, these methods are superior, as they yield all parameters and have distinct accuracy advantages in the presence of noise. Although this is an important realization, additional parameters are required to describe a FFSMS in *free-flying* mode, as for example when it approaches a target.

In this paper, a new parameter identification method is developed, which identifies all inertial parameters needed for the complete reconstruction of a system's *free-flying* joint space dynamics. Novel contributions of the developed methodology include the identification of all system parameters required for the complete reconstruction of a FFSMS in free-flying mode, the use of only manipulator joint torques as system inputs, and its independence of noisy measurements. The identification method is based on a formulation of the system angular momentum conservation during the free-floating mode, and on a kinematics equation with includes a Jacobian. To apply the method, all manipulator joints are commanded to follow optimized exciting trajectories, while the system is in free-floating mode. The methodology is readily applicable to FFSMS with multiple manipulators.

2. Dynamics of free-flying space manipulators

In this section, the dynamics of a FFSMS is presented briefly. Fig. 2 shows a FFSMS consisting of a SC, equipped with thrusters, with N_{rw} RWs, and with n manipulators or appendages with revolute joints, in an open chain kinematic configuration. A captured satellite or space debris is considered as part of the manipulator's last link. The m-th manipulator has N_m links, and the sum of all manipulator links K is

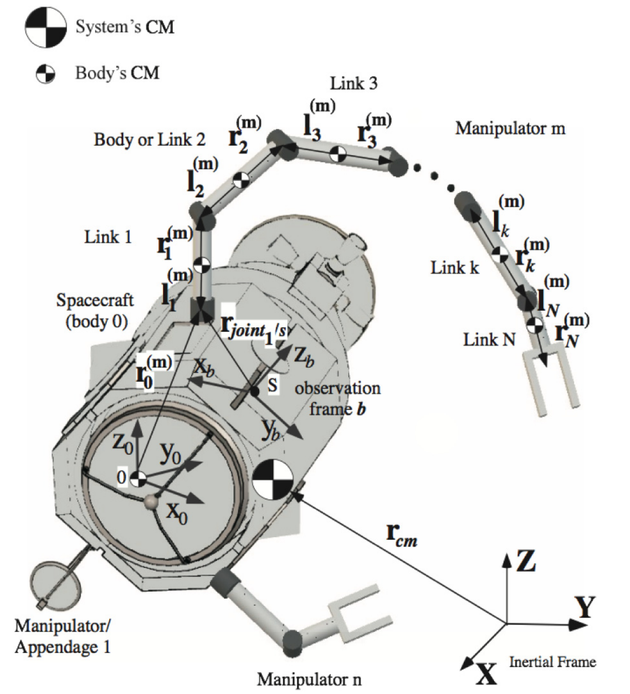

Fig. 2. A free-flying space manipulator system with n manipulators.

$$K = \sum_{m=1}^{n} N_m \tag{1}$$

A frame $\boldsymbol{O}\{\mathbf{x_0},\ \mathbf{y_0},\ \mathbf{z_0}\}$ is attached at the SC center of mass (CM). A SC *feature point* S is tracked, and an observation frame $\boldsymbol{b}\{\mathbf{x}_b,\ \mathbf{y}_b,\ \mathbf{z}_b\}$ is attached to it, with orientation that of frame $\boldsymbol{O}$. Moreover, a frame $\boldsymbol{rw,k}\{\mathbf{x}_{rw,k},\ \mathbf{y}_{rw,k},\ \mathbf{z}_{rw,k}\}$ is attached to the k-th RW. Frame $\boldsymbol{i}\{\mathbf{X},\ \mathbf{Y},\ \mathbf{Z}\}$ is the inertial frame. In this work, the left superscript on $(\bullet)$ indicates the frame in which $(\bullet)$ is projected. A missing left superscript indicates the inertial frame.

2.1. System angular momentum

The *system* angular momentum with respect to the system CM, $\mathbf{h}_{cm}$, is written as the sum of the robotic servicer's angular momentum $\mathbf{h}_{rs}$ and the angular momentum of the RWs due to their relative rotation with respect to the servicer SC, $\mathbf{h}_{rw/sc}$

$$\mathbf{h}_{cm} = \mathbf{h}_{rs} + \mathbf{h}_{rw/sc} \tag{2}$$

The robotic servicer's angular momentum $\mathbf{h}_{rs}$ is given by [23]

$$\mathbf{h}_{rs} = \mathbf{R_0}({}^{\mathbf{0}}\mathbf{D}\,{}^{\mathbf{0}}\boldsymbol{\omega}_{\mathbf{0}} + {}^{\mathbf{0}}\mathbf{D}_q\,\dot{\mathbf{q}}) \tag{3}$$

where ${}^{\mathbf{0}}\boldsymbol{\omega}_{\mathbf{0}}$ is the SC angular velocity. The column vector $\dot{\mathbf{q}}$ is

$$\dot{\mathbf{q}} = [\dot{\mathbf{q}}^{(1)\mathrm{T}} \quad \cdots \quad \dot{\mathbf{q}}^{(m)\mathrm{T}} \quad \cdots \quad \dot{\mathbf{q}}^{(n)\mathrm{T}}]^{\mathrm{T}} \tag{4}$$

where the $N_m\ x\ 1$ column-vector $\dot{\mathbf{q}}^{(m)}$ represents the joint rates vector of the m-th manipulator. The matrix $\mathbf{R_0}$ is the rotation matrix that describes the orientation of frame $\boldsymbol{O}$ with respect to the inertial frame, expressed as a function of the Euler parameters $\boldsymbol{\varepsilon}$, η. The inertia-type matrices ${}^{\mathbf{0}}\mathbf{D}$, ${}^{\mathbf{0}}\mathbf{D}_q$ are given in [21]; the inertial parameters of the RWs are considered as part of the SC inertial parameters. In contrast to [19], in this formulation, the servicer's angular momentum is not a function of the SC linear velocity.

The angular momentum of the RWs due to their relative rotation with respect to the servicer's SC, $\mathbf{h}_{rw/sc}$, is given by

$$\mathbf{h}_{rw/sc} = \mathbf{R_0} \sum_{i=1}^{N_{rw}} {}^{\mathbf{0}}\mathbf{a}_{rw,i} I_{rw,i} \dot{q}_{rw,i} = \mathbf{R_0}{}^{\mathbf{0}}\mathbf{A}_{rw}\dot{\mathbf{q}}_{rw} = \mathbf{A}_{rw}\dot{\mathbf{q}}_{rw} \tag{5}$$

where $I_{rw,i}$ is the i-th RW's polar moment of inertia, ${}^{\mathbf{0}}\mathbf{a}_{rw,i}$ is the vector that denotes the i-th RW's rotation axis, $\dot{q}_{rw,i}$ is the i-th RW's spin rate with respect to its stator, $\dot{\mathbf{q}}_{rw}$ is the column vector of the RWs relative angular rates, and the inertia-type matrix ${}^{\mathbf{0}}\mathbf{A}_{rw}$ is an appropriate matrix.

2.2. Equations of motion of FFSMS

For FFSMS, the Lagrangian L can be assumed to be equal to the system kinetic energy T. This energy is written as

$$\begin{aligned} T \;=\; & \frac{1}{2} M {}^{\mathbf{0}}\dot{\mathbf{r}}_{cm}^{\mathrm{T}} {}^{\mathbf{0}}\dot{\mathbf{r}}_{cm} + \frac{1}{2} {}^{\mathbf{0}}\boldsymbol{\omega}_{\mathbf{0}}^{\mathrm{T}} {}^{\mathbf{0}}\mathbf{D} {}^{\mathbf{0}}\boldsymbol{\omega}_{\mathbf{0}} + {}^{\mathbf{0}}\boldsymbol{\omega}_{\mathbf{0}}^{\mathrm{T}} {}^{\mathbf{0}}\mathbf{D}_q \dot{\mathbf{q}} + \frac{1}{2}\dot{\mathbf{q}}^{\mathrm{T}} {}^{\mathbf{0}}\mathbf{D}_{qq}\dot{\mathbf{q}} \\ & + {}^{\mathbf{0}}\boldsymbol{\omega}_{\mathbf{0}}^{\mathrm{T}} {}^{\mathbf{0}}\mathbf{A}_{rw}\dot{\mathbf{q}}_{rw} + \frac{1}{2}\dot{\mathbf{q}}_{rw}^{\mathrm{T}} {}^{\mathbf{0}}\mathbf{I}_{rw}\dot{\mathbf{q}}_{rw} \end{aligned} \tag{6}$$

where M is the system total mass, ${}^{\mathbf{0}}\dot{\mathbf{r}}_{cm}$ is the system CM linear velocity, inertia-type matrices ${}^{\mathbf{0}}\mathbf{D}$, ${}^{\mathbf{0}}\mathbf{D}_q$, and ${}^{\mathbf{0}}\mathbf{D}_{qq}$ are given in [21] and inertia-type matrix ${}^{\mathbf{0}}\mathbf{I}_{rw}$ is given by

$${}^{\mathbf{0}}\mathbf{I}_{rw} = diag\left(I_{rw,1}, \ldots, I_{rw,N_{rw}}\right) \tag{7}$$

The first four terms of the kinetic energy in (6) have been presented in [23]. The two additional terms refer to the kinetic energy due to the presence of rotating RWs on the SC.

Using the generalized speeds [23]

$${}^{\mathbf{0}}\mathbf{v} = [{}^{\mathbf{0}}\dot{\mathbf{r}}_{cm}^{\mathrm{T}} \quad {}^{\mathbf{0}}\boldsymbol{\omega}_{\mathbf{0}}^{\mathrm{T}} \quad \dot{\mathbf{q}}^{\mathrm{T}} \quad \dot{\mathbf{q}}_{rw}^{\mathrm{T}}]^{\mathrm{T}} \tag{8}$$

and employing a quasi-coordinate formulation yields [24],

$$\frac{d}{dt}\left(\frac{\partial T}{\partial {}^{\mathbf{0}}\dot{\mathbf{r}}_{cm}}\right) + {}^{\mathbf{0}}\boldsymbol{\omega}_{\mathbf{0}}^{\times}\frac{\partial T}{\partial {}^{\mathbf{0}}\dot{\mathbf{r}}_{cm}} = {}^{\mathbf{0}}\mathbf{f}_{\mathbf{0}} \tag{9}$$

$$\frac{d}{dt}\left(\frac{\partial T}{\partial {}^{\mathbf{0}}\boldsymbol{\omega}_{\mathbf{0}}}\right) + {}^{\mathbf{0}}\boldsymbol{\omega}_{\mathbf{0}}^{\times}\frac{\partial T}{\partial {}^{\mathbf{0}}\boldsymbol{\omega}_{\mathbf{0}}} + {}^{\mathbf{0}}\dot{\mathbf{r}}_{cm}^{\times}\frac{\partial T}{\partial {}^{\mathbf{0}}\dot{\mathbf{r}}_{cm}} = {}^{\mathbf{0}}\mathbf{n}_{\mathbf{0}} \tag{10}$$

$$\frac{d}{dt}\left(\frac{\partial T}{\partial \dot{\mathbf{q}}}\right) - \frac{\partial T}{\partial \mathbf{q}} = \boldsymbol{\tau}_{K\times 1} \tag{11}$$

$$\frac{d}{dt}\left(\frac{\partial T}{\partial \dot{\mathbf{q}}_{rw}}\right) = \boldsymbol{\tau}_{rw_{N_{rw}\times 1}} \tag{12}$$

where $(*)^{\times}$ denotes the skew symmetric matrix, $\mathbf{f_0}$ is the resulting external force applied to the SC by its thrusters, $\mathbf{n_0}$ is the associated moment, $\boldsymbol{\tau}$ is the vector of manipulators joint torques, and $\boldsymbol{\tau}_{rw}$ is the vector of RWs torques.

Eqs. (9)–(12) can be written in matrix form as

$${}^{\mathbf{0}}\mathbf{H}^{+}(\mathbf{q}){}^{\mathbf{0}}\dot{\mathbf{v}} + {}^{\mathbf{0}}\mathbf{c}^{+}(\mathbf{q}, \dot{\mathbf{q}}, \dot{\mathbf{q}}_{rw}, {}^{\mathbf{0}}\dot{\mathbf{r}}_{cm}, {}^{\mathbf{0}}\,\boldsymbol{\omega}_{\mathbf{0}}) = {}^{\mathbf{0}}\mathbf{Q} \tag{13}$$

where ${}^{\mathbf{0}}\dot{\mathbf{v}}$ is the derivative of ${}^{\mathbf{0}}\mathbf{v}$ in frame ***0***, and ${}^{\mathbf{0}}\mathbf{H}^{+}$ is the $(6+K+N_{rw}) \times (6+K+N_{rw})$ positive definite symmetric system inertia matrix, given by

$${}^{\mathbf{0}}\mathbf{H}^{+} = \begin{bmatrix} M\mathbf{1} & \mathbf{0} & \mathbf{0} & \mathbf{0} \\ \mathbf{0} & {}^{\mathbf{0}}\mathbf{D} & {}^{\mathbf{0}}\mathbf{D}_q & {}^{\mathbf{0}}\mathbf{A}_{rw} \\ \mathbf{0} & {}^{\mathbf{0}}\mathbf{D}_q^{\mathrm{T}} & {}^{\mathbf{0}}\mathbf{D}_{qq} & \mathbf{0} \\ \mathbf{0} & {}^{\mathbf{0}}\mathbf{A}_{rw}^{\mathrm{T}} & \mathbf{0} & {}^{\mathbf{0}}\mathbf{I}_{rw} \end{bmatrix} \tag{14}$$

Vector ${}^{\mathbf{0}}\mathbf{c}^{+}$ contains the remaining nonlinear terms of the left-hand-side of Eqs. (9)–(12), and the vector of generalized forces ${}^{\mathbf{0}}\mathbf{Q}$ can be written as in [25]

$${}^{\mathbf{0}}\mathbf{Q} = \begin{bmatrix} \mathbf{0}_{3\times 1} \\ \mathbf{0}_{3\times 1} \\ \boldsymbol{\tau}_{K\times 1} \\ \boldsymbol{\tau}_{rw_{N_{rw}\times 1}} \end{bmatrix} + \sum_{p=1}^{i_f} {}^{\mathbf{0}}\mathbf{J}_{\mathbf{0},p}^{\mathrm{T}} {}^{\mathbf{0}}\mathbf{F}_{\mathbf{0},p} + \sum_{m=1}^{n}\sum_{i=1}^{N_m}\sum_{p=1}^{i_f} {}^{\mathbf{0}}\mathbf{J}_{i,p}^{(m)\mathrm{T}} {}^{\mathbf{0}}\mathbf{F}_{i,p}^{(m)} \tag{15}$$

where ${}^{\mathbf{0}}\mathbf{F}_{\mathbf{0},p}$ is the p-th external force/moment applied to the SC by its thrusters, with ${}^{\mathbf{0}}\mathbf{J}_{\mathbf{0},p}$ the corresponding Jacobian matrix, ${}^{\mathbf{0}}\mathbf{F}_{i,p}^{(m)}$ is the p-th external force/moment applied to the i-th body of the m-th manipulator, and ${}^{\mathbf{0}}\mathbf{J}_{i,p}^{(m)}$ is the corresponding Jacobian matrix, and i_f is the number of applied forces/moments on the corresponding body. Jacobian matrices $\mathbf{J}_{\mathbf{0},p}$ and $\mathbf{J}_{i,p}^{(m)}$ are given in [26] and Appendix.

3. The parameter identification method

In our previous work [21], a parameter identification method was proposed that identifies a minimal vector of parameters $\boldsymbol{\pi}$ required in the reconstruction of the *free-floating* joint space dynamics. Nevertheless, missions with a robotic servicer in free-flying or attitude control mode require accurate knowledge of the *free-flying* joint space dynamics; however, the corresponding parameter sets are not identical. In the free-flying mode, the required parameters are those that can reconstruct $\mathbf{H}^{+}$, $\mathbf{c}^{+}$, $\mathbf{J}_{\mathbf{0},p}$ and $\mathbf{J}_{i,p}^{(m)}$ in joint space dynamics in Eq. (13). The vector of parameters $\boldsymbol{\pi}$ identified in [21] allows partial reconstruction of these; therefore additional parameters must be estimated. In particular, for matrix $\mathbf{H}^{+}$ and vector $\mathbf{c}^{+}$, the system total mass M is required also, while for matrices $\mathbf{J}_{\mathbf{0},p}$ and $\mathbf{J}_{i,p}^{(m)}$, a vector of additional parameters $\boldsymbol{\varphi}$ must be available. Specifically, the equations of motion of a FFSMS as a function of the inertial parameters are

$$\begin{bmatrix} M\mathbf{1} & \mathbf{0} & \mathbf{0} & \mathbf{0} \\ \mathbf{0} & {}^{\mathbf{0}}\mathbf{D}(\boldsymbol{\pi}) & {}^{\mathbf{0}}\mathbf{D}_q(\boldsymbol{\pi}) & {}^{\mathbf{0}}\mathbf{A}_{rw} \\ \mathbf{0} & {}^{\mathbf{0}}\mathbf{D}_q^{\mathrm{T}}(\boldsymbol{\pi}) & {}^{\mathbf{0}}\mathbf{D}_{qq}(\boldsymbol{\pi}) & \mathbf{0} \\ \mathbf{0} & {}^{\mathbf{0}}\mathbf{A}_{rw}^{\mathrm{T}} & \mathbf{0} & {}^{\mathbf{0}}\mathbf{I}_{rw} \end{bmatrix} {}^{\mathbf{0}}\dot{\mathbf{v}} + {}^{\mathbf{0}}\mathbf{c}^{+}(M, \boldsymbol{\pi}) = {}^{\mathbf{0}}\mathbf{Q}(\boldsymbol{\pi}, \boldsymbol{\varphi}) \tag{16}$$

The identification method developed here is based on angular momentum and kinematics equation sets. The first set is used for identifying vector $\boldsymbol{\pi}$, while the second one for identifying vector $\boldsymbol{\varphi}$. Once vectors $\boldsymbol{\pi}$ and $\boldsymbol{\varphi}$ become available, one can easily reconstruct the total mass M. Note that during the identification experiment, thrusters and reaction wheels are off. Hence the system operates in *free-floating* mode; however, the parameters identified by the identification method render the *free-flying* dynamics fully known.

In the free-floating mode, the system angular momentum and the system linear velocity remain constant

$$\mathbf{h}_{cm} = (\mathbf{h}_{cm})_{in} = const. \tag{17}$$

$$\dot{\mathbf{r}}_{cm} = (\dot{\mathbf{r}}_{cm})_{in} = const. \tag{18}$$

where $(*)_{in}$ is the initial value of $(*)$.

A flowchart for the implementation of the developed method in five steps is shown in Fig. 3. During the procedure, manipulator joints follow appropriate exciting trajectories.

3.1. Identification based on the angular momentum principle

To use Eq. (2) for parameter identification, the RWs relative angular momentum with respect to the SC, ${}^{\mathbf{0}}\mathbf{h}_{rw/sc}$, must be known. This is the case, as the RWs moments of inertia, their location with respect to SC frame and the RW joints rates are practically known from their specifications, their mounting procedure and the RWs encoders respectively. The robotic servicer's angular momentum, $\mathbf{h}_{rs}$, must be expressed linearly with respect to a minimal inertial parameter vector $\boldsymbol{\pi}$ [21]. Thus, the servicer's angular momentum can be written as

$$\mathbf{h}_{rs} = \mathbf{Y}(\dot{\mathbf{q}},\ \mathbf{q},\ \boldsymbol{\omega}_{\mathbf{0}},\ \boldsymbol{\varepsilon},\ \eta)\,\boldsymbol{\pi} \tag{19}$$

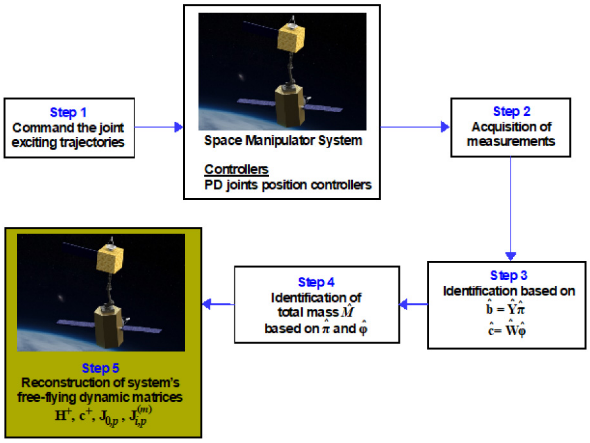

Fig. 3. Flow chart for the implementation of the proposed method.

where the $3 \times k$ matrix $\mathbf{Y}$ is the regressor matrix, and k is the dimension of $\boldsymbol{\pi}$. In contrast to other methods that require joint accelerations and spacecraft angular acceleration, the key feature of this regressor is that it does *not* require noisy acceleration measurements. Specifically, joint accelerations are more noisy than joint rates since the former are obtained by the differentiation of the latter. Also, spacecraft angular accelerations are more noisy for the same reason. Therefore, eliminating both accelerations and their large associated noise improves significantly the quality of the identification results of the developed method.

Initially, the robotic servicer and its RWs each have accumulated angular momentum

$$(\mathbf{h}_{cm})_{in} = (\mathbf{h}_{rs})_{in} + \left(\mathbf{h}_{rw/sc}\right)_{in} \tag{20}$$

Based on Eqs. (19), (20) becomes,

$$(\mathbf{h}_{cm})_{in} = (\mathbf{Y})_{in}\,\boldsymbol{\pi} + \left(\mathbf{h}_{rw/sc}\right)_{in} \tag{21}$$

Based on Eqs. (21), (17) becomes

$$\mathbf{h}_{cm} = \mathbf{Y}\boldsymbol{\pi} + \mathbf{h}_{rw/sc} = (\mathbf{Y})_{in}\,\boldsymbol{\pi} + \left(\mathbf{h}_{rw/sc}\right)_{in} \tag{22}$$

This equation can be written further as

$$\left(\mathbf{Y} - (\mathbf{Y})_{in}\right)\boldsymbol{\pi} = \left(\mathbf{h}_{rw/sc}\right)_{in} - \mathbf{h}_{rw/sc} \tag{23}$$

Assuming N measurements of the variables $(\dot{\mathbf{q}}, \mathbf{q}, \dot{\mathbf{q}}_{rw}, \boldsymbol{\omega}_0)$, and $\boldsymbol{\varepsilon}, \eta$ obtained at time instants $t_1, t_2, \ldots, t_N$ during manipulator motion, Eq. (23) results in the following system of equations

$$\hat{\mathbf{b}} = \begin{bmatrix} \left(\mathbf{h}_{rw/sc}\right)_{in} - \mathbf{h}_{rw/sc}(t_1) \\ \left(\mathbf{h}_{rw/sc}\right)_{in} - \mathbf{h}_{rw/sc}(t_2) \\ \vdots \\ \left(\mathbf{h}_{rw/sc}\right)_{in} - \mathbf{h}_{rw/sc}(t_N) \end{bmatrix} = \begin{bmatrix} \mathbf{Y}(t_1) - (\mathbf{Y})_{in} \\ \mathbf{Y}(t_2) - (\mathbf{Y})_{in} \\ \vdots \\ \mathbf{Y}(t_N) - (\mathbf{Y})_{in} \end{bmatrix} \boldsymbol{\pi} = \hat{\mathbf{Y}}\boldsymbol{\pi} \tag{24}$$

All required quantities, can be obtained directly or indirectly using available sensors. The required joint angles $\mathbf{q}$ are obtained directly by the joint motor encoders, while the joint rates $\dot{\mathbf{q}}$ and the RW rates $\dot{\mathbf{q}}_{rw}$ are obtained by differentiating $\mathbf{q}$ and $\mathbf{q}_{rw}$, available directly from the corresponding encoders. Note that RWs joint rates measurements are required only before the identification experiment. The orientation of the servicer's SC, and thus, the corresponding Euler parameters $\boldsymbol{\varepsilon}$, η, can be obtained directly using Star or Sun Trackers, or indirectly using installed IMUs, while ${}^{\mathbf{0}}\boldsymbol{\omega}_{\mathbf{0}}$ can be provided by IMUs also.

Note that if the robotic servicer is initially at rest and its RWs have accumulated angular momentum, (a realistic scenario following a stabilization procedure), Eq. (24) still holds with $(\mathbf{Y})_{in} = \mathbf{0}$. If both the robotic servicer and its RWs are initially at rest, and hence $(\mathbf{h}_{cm})_{in} = \mathbf{0}$, then angular momentum must be introduced in the RWs. This can be implemented using a speed controller and RWs desired rates $\left(\dot{\mathbf{q}}_{rw}\right)_{des}$. Once the desired rates are reached, the RWs spin with the desired accumulated relative angular momentum

$$\left(\mathbf{h}_{rw/sc}\right)_{des} = \mathbf{A}_{rw}\left(\dot{\mathbf{q}}_{rw}\right)_{des} \tag{25}$$

Then, the RWs controller is turned off and all manipulator joints are commanded to follow optimized exciting trajectories, while the system is in free-floating mode.

Then, Eq. (24) still holds with

$$\left(\mathbf{h}_{rw/sc}\right)_{in} = \left(\mathbf{h}_{rw/sc}\right)_{des} \tag{26}$$

3.2. Identification based on kinematics

To estimate the vector of parameters $\boldsymbol{\varphi}$, a kinematic equation that includes the Jacobian matrix $\mathbf{J}_{0,p}$ is used. Specifically, the linear velocity of an arbitrary point P on the SC and the SC angular velocity can be related to the time derivative of generalized speeds through the Jacobian matrix $\mathbf{J}_{0,p}$ [27]. In more detail, for the observation point S on the SC of the FFSMS, see Fig. 2, this kinematic relation is written as

$$\begin{bmatrix} {}^{\mathbf{0}}\dot{\mathbf{r}}_s \\ {}^{\mathbf{0}}\boldsymbol{\omega}_{\mathbf{0}} \end{bmatrix} = {}^{\mathbf{0}}\mathbf{J}_{0,s}\,{}^{\mathbf{0}}\mathbf{v} \tag{27}$$

Using (A.3),

$${}^{\mathbf{0}}\dot{\mathbf{r}}_s - {}^{\mathbf{0}}\dot{\mathbf{r}}_{cm} = {}^{\mathbf{0}}\mathbf{J}_1^{(0)}\,{}^{\mathbf{0}}\boldsymbol{\omega}_{\mathbf{0}} + {}^{\mathbf{0}}\mathbf{J}_2^{(0)}\dot{\mathbf{q}} \tag{28}$$

where $\mathbf{J}_1^{(0)}$ and $\mathbf{J}_2^{(0)}$ are submatrices of the $\mathbf{J}_{0,s}$, given in [26]. The right side of (28) can be formulated as

$${}^{\mathbf{0}}\dot{\mathbf{r}}_s - {}^{\mathbf{0}}\dot{\mathbf{r}}_{cm} = \mathbf{W}\left(\dot{\mathbf{q}},\, \mathbf{q},\, {}^{\mathbf{0}}\boldsymbol{\omega}_{\mathbf{0}}\right)\boldsymbol{\varphi} + \mathbf{x}\left({}^{\mathbf{0}}\boldsymbol{\omega}_{\mathbf{0}},\, {}^{\mathbf{0}}\mathbf{r}_{joint_1/s}\right) \tag{29}$$

where $\mathbf{W}$ contains measurable variables, ${}^{\mathbf{0}}\mathbf{r}_{joint_1/s}$ is the known position vector from the tracked point S to a manipulator's first joint expressed in frame ***0***, see Fig. 2, and $\mathbf{x}$ contains both measurable ${}^{\mathbf{0}}\boldsymbol{\omega}_{\mathbf{0}}$ and known quantity ${}^{\mathbf{0}}\mathbf{r}_{joint_1/s}$. This equation can be further written as

$${}^{\mathbf{0}}\dot{\mathbf{r}}_s = \mathbf{W}\left(\dot{\mathbf{q}},\, \mathbf{q},\, {}^{\mathbf{0}}\boldsymbol{\omega}_{\mathbf{0}}\right)\boldsymbol{\varphi} + \mathbf{R}_{\mathbf{0}}^{\mathrm{T}}\dot{\mathbf{r}}_{cm} + \mathbf{x}\left({}^{\mathbf{0}}\boldsymbol{\omega}_{\mathbf{0}},\, {}^{\mathbf{0}}\mathbf{r}_{joint_1/s}\right) \tag{30}$$

The $3 \times l$ matrix $\mathbf{W}$ is the regressor matrix corresponding to the vector of inertial parameters $\boldsymbol{\varphi}$ and l is the dimension of $\boldsymbol{\varphi}$. The system CM linear velocity $\dot{\mathbf{r}}_{cm}$ is constant in free-floating mode, see (18), and unknown; hence, it can be included in the vector to be estimated. Note that this regressor too, does *not* require acceleration measurements and it applies to *multi-arm* systems. As discussed earlier, elimination of linear and angular accelerations improves the quality of the identification results. Also, the spacecraft linear velocity is needed here only in (30), and is less noisy with respect to the linear acceleration, since the former is obtained by integration.

Obtaining again N measurements of $\dot{\mathbf{r}}_s$, $\dot{\mathbf{q}}$, $\mathbf{q}$, $\boldsymbol{\omega}_{\mathbf{0}}$, $\boldsymbol{\varepsilon}$, η at time instants $t_1, t_2, \ldots, t_N$ during an appropriate trajectory, results in the following system of equations

$$\hat{\mathbf{c}} = \begin{bmatrix} {}^{\mathbf{0}}\dot{\mathbf{r}}_s(t_1) - \mathbf{x}(t_1) \\ {}^{\mathbf{0}}\dot{\mathbf{r}}_s(t_2) - \mathbf{x}(t_2) \\ \vdots \\ {}^{\mathbf{0}}\dot{\mathbf{r}}_s(t_N) - \mathbf{x}(t_N) \end{bmatrix} = \begin{bmatrix} \mathbf{W}(t_1) & \mathbf{R}_{\mathbf{0}}^{\mathrm{T}} \\ \mathbf{W}(t_2) & \mathbf{R}_{\mathbf{0}}^{\mathrm{T}} \\ \vdots & \vdots \\ \mathbf{W}(t_N) & \mathbf{R}_{\mathbf{0}}^{\mathrm{T}} \end{bmatrix} \begin{bmatrix} \boldsymbol{\varphi} \\ \dot{\mathbf{r}}_{cm} \end{bmatrix} = \hat{\mathbf{W}} \begin{bmatrix} \boldsymbol{\varphi} \\ \dot{\mathbf{r}}_{cm} \end{bmatrix} \tag{31}$$

The additional measurement of the SC linear velocity can be obtained by fusing GNSS, inertial, and magnetometer data [28]. To obtain good identification results, the manipulators must follow sufficiently exciting trajectories, also see Section 3.4.

The systems of equations given by Eqs. (24) and (31), are over-determined and therefore, their solution is obtained by appropriate recursive or non-recursive algorithms (e.g. least squares). The regressor matrices must be of full rank for Eqs. (24) and (31) to be solved for $\boldsymbol{\pi}$ and $\boldsymbol{\varphi}$, which in turn requires that $\boldsymbol{\pi}$ and $\boldsymbol{\varphi}$ are minimal parameter sets, obtained as in [21].

3.3. System total mass estimation

Based on the identified vector parameters $\boldsymbol{\pi}$ and $\boldsymbol{\varphi}$, the total mass M can be estimated using various expressions of the form

$$M = \pi_i / \left(\varphi_j \varphi_k\right) \tag{32}$$

where i, j, k can be easily selected based on the fact that some of the π_i's are related to a product of two φ_i's. One of these expressions is adequate for the total mass calculation. Vector parameters $\boldsymbol{\pi}$ and $\boldsymbol{\varphi}$ together with the total mass M are enough to reconstruct the system's free-flying dynamics.

For a FFSMS, Eq. (32) is applicable and preferable since it does not require additional steps in the identification procedure. However, Eq. (32) may be sensitive to sensor noise in case of small mass systems such as the autonomous robot *Cepheus*, part of our Space Robot Emulator, especially if low cost sensors are used. For such cases an additional identification step is proposed, which is applicable before the robot performs the joint trajectories. Locking all joints, the entire space manipulator system becomes an equivalent to a single body. Then, external forces are applied to the system at time t_1 for a time interval Δt. The total mass M is identified by measuring the CM velocity at time instants t_1 and $t_2 = t_1 + \Delta t$, as follows.

The system linear momentum vector $\mathbf{p}$ is given by

$$\mathbf{p} = M\dot{\mathbf{r}}_{cm} \tag{33}$$

The rate of change of the linear momentum is given by

$$\dot{\mathbf{p}} = \boldsymbol{\Sigma}\mathbf{F} \tag{34}$$

where $\boldsymbol{\Sigma}\mathbf{F}$ is the sum of the forces acting on the body. Integration of (34), yields the linear momentum at t_2,

$$\mathbf{p}_{t_2} = \mathbf{p}_{t_1} + \int_{t_1}^{t_2} \boldsymbol{\Sigma}\mathbf{F} dt \tag{35}$$

where $\mathbf{p}_{t_1}$ and $\mathbf{p}_{t_2}$ are the system linear momentum at time instants t_1 and t_2, respectively. Substituting (33) to (35) yields

$$M\dot{\mathbf{r}}_{cm|t_2} = M\dot{\mathbf{r}}_{cm|t_1} + \int_{t_1}^{t_2} \boldsymbol{\Sigma}\,\mathbf{F} dt \tag{36}$$

where $\dot{\mathbf{r}}_{cm|t_1}$ and $\dot{\mathbf{r}}_{cm|t_2}$ are the linear velocities of body's CM at time instants t_1 and t_2, respectively. To facilitate the estimation of M, constant external forces can be applied. Thus, (36) is simplified further as follows

$$M\dot{\mathbf{r}}_{cm|t_2} = M\dot{\mathbf{r}}_{cm|t_1} + \boldsymbol{\Sigma}\mathbf{F}\Delta t \tag{37}$$

The linear velocity of the observation point S on the spacecraft, whose motion can be tracked, is expressed as

$$\dot{\mathbf{r}}_s = \dot{\mathbf{r}}_{cm} + \boldsymbol{\omega} \times (\mathbf{r}_s - \mathbf{r}_{cm}) \tag{38}$$

where $\boldsymbol{\omega}$ is the angular velocity of the equivalent single body. If the spacecraft attitude is maintained constant, for example using reaction wheels, then (38) results in

$$\dot{\mathbf{r}}_s = \dot{\mathbf{r}}_{cm} \tag{39}$$

and therefore, $\dot{\mathbf{r}}_{cm}$ is known. Also, the thruster forces $\boldsymbol{\Sigma}\mathbf{F}$ acting on the equivalent single body are known since they are set. Then, using (37) and (39), the system total mass can be identified using data from any axis, e.g. for the Y-axis, as

$$M = \frac{\Sigma F_y \Delta t}{\left(\dot{r}_{s|t_2}\right)_y - \left(\dot{r}_{s|t_1}\right)_y} \tag{40}$$

In (40) noisy acceleration measurements are *not* used.

3.4. Exciting trajectories

Appropriate exciting trajectories are required that result in $\hat{\mathbf{Y}}$ and $\hat{\mathbf{W}}$ being of full rank and with a small condition number. A small condition number is needed so that the estimation is more accurate and reasonably insensitive to noise. The developed exciting trajectories are based on truncated Fourier series. To satisfy desired initial and final conditions, a fifth-order polynomial is added to truncated Fourier series

$$q_i^{(m)} = \sum_{l=1}^{N_f} \frac{a_l^{i(m)}}{\omega_f l} \sin\left(\omega_f l t\right) - \frac{b_l^{i(m)}}{\omega_f l} \cos\left(\omega_f l t\right) + \sum_{j=0}^{5} c_j^{i(m)} t^j \tag{41}$$

where $q_i^{(m)}$ represents the i-th joint angle of the m-th manipulator, $m = 1, \ldots, n$, $i = 1, \ldots, N_m$, N_f is the number of the harmonics employed, $a_l^{i(m)}$ and $b_l^{i(m)}$ are free coefficients, $c_j^{i(m)}$ are polynomial coefficients to be determined using the desired initial and final conditions and the free-coefficients, and $\omega_f = 2\pi/t_f$ with t_f the motion duration.

The free coefficients of the Fourier series are found by minimizing the condition number of the regressor matrix $\hat{\mathbf{Y}}$. These also yield a small condition number for the regressor matrix $\hat{\mathbf{W}}$. The optimization algorithm is implemented using the Global Search Solver provided by the Global Optimization Toolbox (MathWorks), considering mechanical constraints on joint positions and velocities.

3.5. Noise modeling

To identify the required parameters, measurements obtained by the system sensors must be available. Here, it is assumed that an Inertial Measurement Unit (IMU) and joint encoders are available on an FFSMS. For the IMU's gyro and the acceleration measurements, angle random walk $0.01\ ^\circ/\sqrt{h}$, bias instability $0.3\ ^\circ/h$, and velocity random walk $0.001\ (m/s)/\sqrt{h}$ and bias instability $10\ \mu g$, were considered respectively. Sampling time was chosen to be 50 *ms*. The sensor was modeled in the Matlab Navigation Toolbox using the imuSensor object and the function imu().

Encoders on the FFSMS and RWs motors are used with the noise on the measured angle to be zero mean Gaussian noise with standard deviation 2.5e−5 *rad*.

4. Simulation results

In this section, the proposed identification method is illustrated using a spatial servicer with a three degrees-of-freedom (DoF) manipulator with revolute joints, in an open chain kinematic configuration. The servicer parameters are given in Table 1. The studied SC is assumed to have three RWs in an orthogonal configuration with $I_{rw,i} = 0.18\ kg\ m^2$. The size of the minimum set of parameters $\boldsymbol{\pi}$ for this system is nineteen, given in [21], while for $\boldsymbol{\varphi}$ is five. These are given in Appendix.

The duration of the first simulation is $t_f = 80\ s$, and $N_f = 3$. The desired initial and final conditions correspond to zero joint angles, rates and accelerations. All measurements are sampled

Table 1
System parameters of simulation study (SI Units).

i	l_i	r_i	m_i	$(I_{xx})_i$	$(I_{yy})_i$	$(I_{zz})_i$
0	–	$[-1.06, -1.06, 0.67]^{\mathrm{T}}$	1000	600	600	900
1	0.25	0.25	10	0.21	0.21	0.01
2	1.0	1.0	50	0.05	16.69	16.69
3	1.0	1.0	50	0.05	16.69	16.69

Table 2
Optimized trajectory coefficients.

Coeff.	Value	Coeff.	Value	Coeff.	Value
a_1^1	0.0411	a_2^1	−0.0622	a_3^1	0.0002
a_1^2	0.0435	a_2^2	−0.0407	a_3^2	−0.1253
a_1^3	0.0516	a_2^3	−0.0423	a_3^3	0.1343
b_1^1	0.0533	b_2^1	−0.1269	b_3^1	0.0171
b_1^2	−0.0393	b_2^2	0.0596	b_3^2	−0.0444
b_1^3	−0.0153	b_2^3	0.0449	b_3^3	0.0463

Table 3
Initial conditions for simulation study.

Spacecraft angular velocity	$[0.01\ 0.03\ 0.025]^{\mathrm{T}}$ *rad/s*
Spacecraft orientation	$[0.2\ 0.1\ 0.3\ 0.93]^{\mathrm{T}}$
Joint angles and rates	$[0\ 0\ 0]^{\mathrm{T}}$ *rad* $[0\ 0\ 0]^{\mathrm{T}}$ *rad/s*
Angular momentum ${}^{\mathbf{0}}(\mathbf{h}_{rw/sc})_{in}$	$[50\ 50\ 50]^{\mathrm{T}}$ *Nms*
${}^{\mathbf{0}}\mathbf{r}_{joint_1/s}$	$[0\ 0\ 0]^{\mathrm{T}}$ *m*

at 50 *ms*. The coefficients a_l^i and b_l^i of the optimized exciting joint trajectories for minimum condition number of regressor's condition number, are derived for this study and presented in Table 2. The initial conditions for this experiment are given in Table 3.

Using Eqs. (24) and (31), $\boldsymbol{\pi}$ and $\boldsymbol{\varphi}$ are identified, practically with zero relative error (RE) if no noise exists, and accurately when noise is considered, see Table 4. Based on the identified parameters, the total mass M is estimated using e.g.

$$M = \pi_{18}/\left(\varphi_1\varphi_3\right) = \frac{m_0 m_3 l_3 {}^0r_{0_x}/M}{\left(m_0 {}^0r_{0_x}/M\right)\left(m_3 l_3/M\right)} \tag{42}$$

and the corresponding relative error is practically also zero if no noise exists, and 0.97% in the presence of noise. Parameters π_{18} and φ_1, φ_3 are given in [21] and Appendix. Hence, the proposed method is validated. The identified $\boldsymbol{\pi}$ and $\boldsymbol{\varphi}$ of the spatial FFSMS together with the identified system's total mass M are enough to reconstruct the system's free-flying dynamics, as has been shown in Eq. (16).

5. Experimental identification of a planar SMS

The Space Robot Emulator (SRE) of NTUA's Control Systems Lab consists of the autonomous robot *Cepheus* floating over a blue-black hard rock table, see Figs. 4 and 5, and an optical feedback system. The table exhibits very low surface roughness ($<5\ \mu m$), allowing emulation of zero gravity in two dimensions. The robots float over the hard rock table using three air-bearings. Through the porous air bearing material, pressurized CO_2 is supplied creating a thin film of CO_2 between the robot and the table surface, resulting in frictionless planar motion. The CO_2 is provided to each of the three air-bearings via flexible hoses from a central pressurized CO_2 tank. CO_2 is used also for the operation of the three thrusters pairs. The electronic circuitry controls the gas flow using Pulse Width Modulation (PWM), allowing values of thrust in a continuous range, while using on–off technology, as used in actual space systems. To achieve greater fuel autonomy, a reaction wheel is installed, driven by a DC motor with an

Table 4
Simulation identification of parameter vectors.

Parameter	True value	Estimated value	RE (%) no noise	RE (%) with noise
π_1	843.15	842.81	2e−12	0.04
π_2	−111.75	−111.38	−7e−12	−0.32
π_3	120.82	120.86	3e−11	0.04
π_4	843.15	843.85	2e−12	0.08
π_5	120.82	120.58	2e−11	0.20
π_6	1123.50	1124.70	5e−12	0.11
π_7	310.86	310.13	9e−12	0.23
π_8	310.87	310.42	2e−12	0.14
π_9	−246.37	−245.28	−5e−12	−0.44
π_{10}	246.42	246.01	9e−12	0.17
π_{11}	−64.39	−64.95	−2e−11	−0.88
π_{12}	64.44	64.44	3e−12	0.01
π_{13}	−143.50	−143.26	−1e−13	−0.17
π_{14}	158.56	158.06	1e−12	0.32
π_{15}	−143.50	−143.17	−2e−12	−0.23
π_{16}	−47.83	−47.78	−5e−12	−0.11
π_{17}	52.85	52.54	9e−12	0.58
π_{18}	−47.83	−47.78	2e−12	−0.19
π_{19}	93.24	93.10	−1e−12	0.15
φ_1	−0.96	−0.97	−3e−13	−1.77
φ_2	−0.96	−0.97	−9e−14	−1.28
φ_3	0.05	0.04	1e−12	2.87
φ_4	0.14	0.13	6e−13	2.07
φ_5	−0.56	−0.57	−1e−12	−1.50

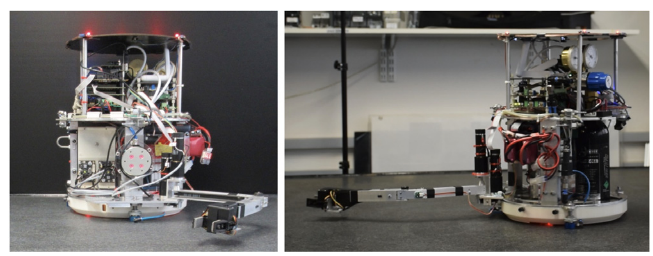

Fig. 4. Autonomous robot Cepheus of NTUA's Space Robot Emulator. (For interpretation of the references to color in this figure legend, the reader is referred to the web version of this article.)

incremental encoder, offering an alternative to the thrusters for attitude control.

The electrical autonomy of the robot is achieved by two Lithium Polymer (Li-Po) batteries, with four cells each. The robot computational system consists of PC-104 boards running Ubuntu with ROS installed, and a Wi-Fi bridge. Finally, the SRE employs an eight-camera PhaseSpace motion capture (mocap) system, providing spacecraft position and orientation feedback.

Cepheus has a two DoF actuated manipulator, see Figs. 4 and 5. Both of its joint motors are equipped with incremental encoders. The feature point on *Cepheus*, S, is the geometrical center of its base (or its SC); an observation frame (frame ***b***) is attached with its origin at S. The frame ***0***, i.e. the frame with origin at the SC CM, has the same orientation with frame ***b***. The mocap system measures the position of point S and the orientation of frame ***b***.

5.1. Identification equations for the planar system

The robotic servicer's angular momentum is written in the form of Eq. (19), which for the planar system reduces to

$$h_{rs_z} = \mathbf{Y}\left(\dot{q}_1, \dot{q}_2, q_1, q_2, \ \omega_{0_z}\right)\boldsymbol{\pi} \tag{43}$$

where q_1, q_2 and $\dot{q}_1$, $\dot{q}_2$ are manipulator joint angles and rates and ω_{0_z} is the SC angular velocity normal to the table.

The kinematic equation for the SC linear velocity, see (30), for the planar case can be written as

$$\dot{\mathbf{r}}_s = \mathbf{W}\left(\dot{q}_1, \dot{q}_2, q_1, q_2, \ \omega_{0_z}, \theta\right)\boldsymbol{\varphi} + \mathbf{x}\left(\omega_{0_z}, \theta, {}^{\mathbf{0}}\mathbf{r}_{joint_1/s}\right) \tag{44}$$

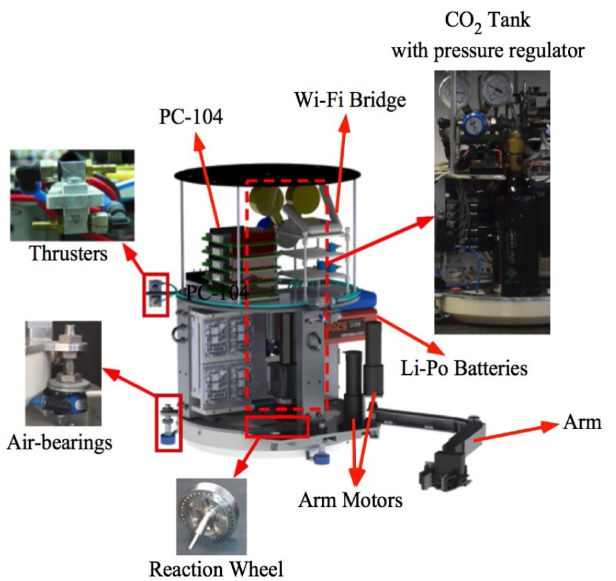

Fig. 5. Cepheus, part of NTUA's Space Robot Emulator. (For interpretation of the references to color in this figure legend, the reader is referred to the web version of this article.)

where θ is the SC orientation (yaw). The vector from point S to the manipulator first joint is ${}^{0}\mathbf{r}_{joint_1/s} = [0.173 \quad 0.091]^{\mathrm{T}}$, and was obtained from the robot CAD model. The minimum set of parameters $\boldsymbol{\pi}$ and $\boldsymbol{\varphi}$ for a planar two DoF manipulator system is eight and four respectively; both are given in Appendix. In the experiment, *Cepheus* and its RW are initially at rest, hence $(\dot{\mathbf{r}}_{cm})_{in} = \mathbf{0}$ and $(h_{cm})_{in} = 0$. Therefore, angular momentum is introduced in the RW. This is implemented by setting the desired RW joint rate $(\dot{q}_{rw})_{des} = -170\ rad/s$ and employing a velocity controller. Hence, given that ${}^{0}A_{rw} = 0.00197\ kg\ m^2$, the desired accumulated angular momentum based on Eq. (25) is

$$\left({}^{0}h_{\mathrm{rw/sc}}\right)_{des} = {}^{0}A_{rw}\,(\dot{q}_{rw})_{des} = -0.3355\ Nms \tag{45}$$

Once RW has the desired angular momentum, the two joints of the manipulator are controlled by PD position controllers to follow the optimized exciting trajectories.

5.2. Optimized joint exciting trajectories

In the identification experiment, $N_f = 3$ and the trajectory duration is $t_f = 20\ s$. The desired initial and final conditions correspond to zero joint angles, rates and accelerations. The mechanical joint constraints satisfied by the optimized trajectories are

$$\begin{aligned} &-1.05 \le q_1 \le 2.50\ [rad] \\ &-2.09 \le q_2 \le 1.40\ [rad] \\ &-0.70 \le \dot{q}_1 \le 0.70\ [rad/s] \\ &-0.50 \le \dot{q}_2 \le 0.50\ [rad/s] \end{aligned} \tag{46}$$

The trajectory coefficients a_l^i and b_l^i are obtained so as to minimize the condition number of $\hat{\mathbf{Y}}$. Here, the condition number was 153. The coefficients are displayed in Table 5.

5.3. Measurements and signal processing

The identification procedure requires measurements of the joint angles and rates, the SC orientation, the SC linear velocity (point S) and the SC angular velocity, all given by the mocap system and encoders. To reduce the effect of noise, appropriate signal processing is employed. The joint angles are filtered and then differentiated; the joint rates are filtered. The position of S and the orientation angle of the SC are differentiated, and the obtained linear and angular velocity are filtered. All filters are low-pass Butterworth filters. The selection of filter cutoff frequencies is based on FFTs. Additional insight about the cutoff frequencies was provided by the FFTs of the signals obtained by the simulated motion of *Cepheus* with approximate CAD parameters.

Table 5
Optimized trajectory coefficients.

Coeff.	Value	Coeff.	Value	Coeff.	Value
a_1^1	−0.025	a_2^1	−0.119	a_3^1	0.100
a_1^2	−0.004	a_2^2	−0.003	a_3^2	0.113
b_1^1	0.007	b_2^1	0.093	b_3^1	−0.158
b_1^2	−0.050	b_2^2	0.126	b_3^2	0.058

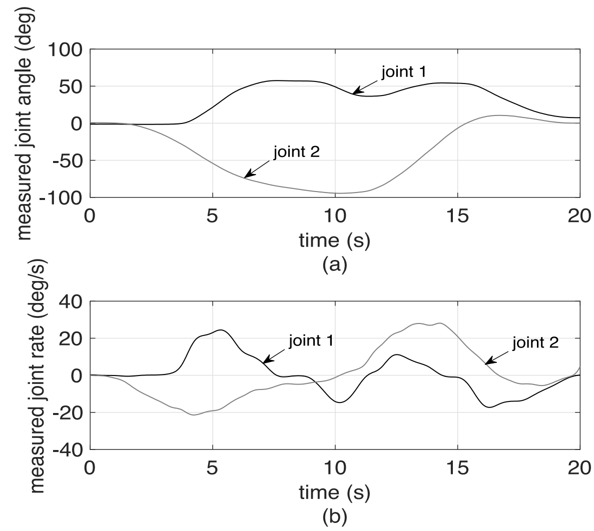

Fig. 6. Measured histories. (a) manipulator joint angles and (b) their rates.

Table 6
Identified vector of parameters $\boldsymbol{\pi}$ and $\boldsymbol{\varphi}$.

Parameter	Value	Parameter	Value
π_1	0.0029	π_5	0.1448
π_2	0.0012	π_6	−0.0018
π_3	−0.0004	π_7	0.0079
π_4	0.0024	π_8	0.0010
φ_1	0.1579	φ_3	0.0020
φ_2	0.0759	φ_4	0.0004

5.4. Experimental identification results for $\boldsymbol{\pi}$ and $\boldsymbol{\varphi}$

Fig. 6 shows the time histories of the experimentally obtained joint angles and rates. Fig. 7 shows the measured SC orientation angle and the SC angular rate, while Fig. 8 shows the SC absolute X and Y positions and velocities. Note that the periodic variations of the position and velocity of the tracked point S are due to the rotation of the robot.

Using the measurements of the joint angles, joint rates and SC orientation, linear and angular velocity, the parameters $\boldsymbol{\pi}$ and $\boldsymbol{\varphi}$ are identified, see Table 6 respectively.

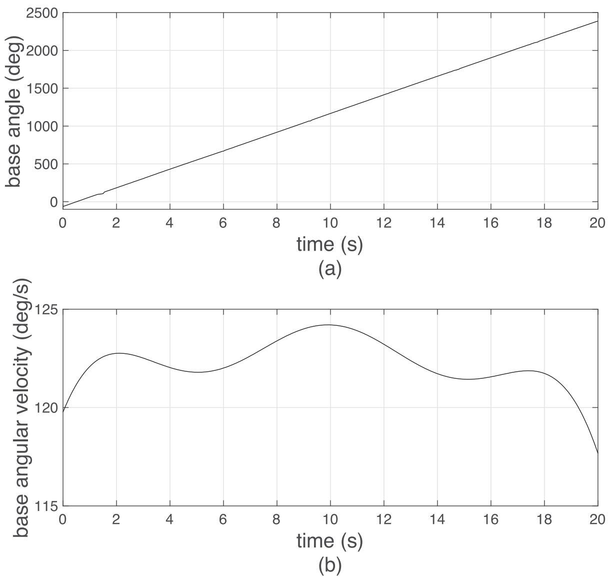

Fig. 7. (a) Measured SC angle and (b) measured SC angular velocity.

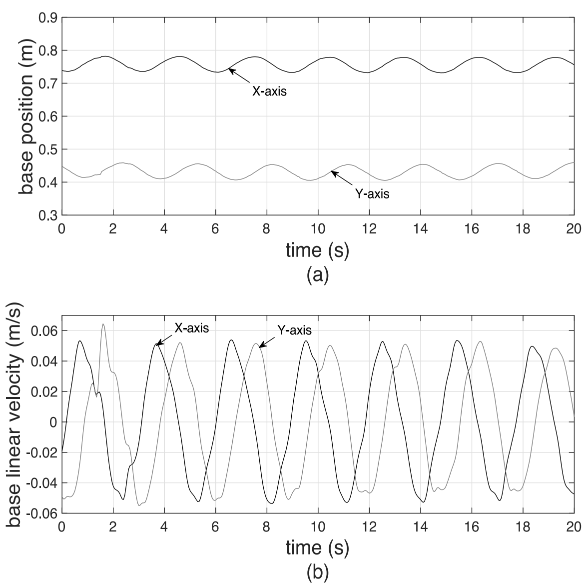

Fig. 8. Measured SC absolute X and Y (a) position and (b) velocity.

5.5. Experimental identification results for the total mass M

For a large mass FFSMS and similar or better sensor technology to the one in the Lab, Eq. (32) is applicable and preferable for the estimation of the system total mass since it does not require the additional step in the identification procedure. However, Eq. (32) may be sensitive to sensor noise in case of small systems such as the autonomous robot *Cepheus*, part of our Space Emulator. In this case, the additional identification step can be employed. Locking all joints, *Cepheus* becomes an equivalent single body. Then, forces generated by thrusters act for a time interval, and the motion of the robot, described by the motion of frame $\boldsymbol{b}$, is captured by the mocap system. Since the thruster orientations with respect to frame $\boldsymbol{b}$ are known, and PWM signals are set and known, the force components ΣF_x, ΣF_y acting on the system CM are known, too. The torque generated by the thrusters is eliminated by the reaction wheel driven by an orientation controller, keeping the

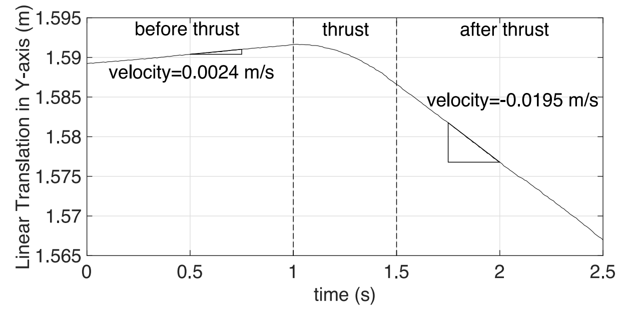

Fig. 9. Linear translation of the robot in Y-axis.

orientation constant. Hence, the total mass of *Cepheus* can be identified using Eq. (40). The velocity $\dot{\mathbf{r}}_s$ in Eq. (40) is obtained by the slopes of the X, Y positions vs. time, using mocap feedback.

To implement this step, all manipulator joints are locked as close as possible to the base, and an orientation PD controller is employed, with gains selected experimentally as $k_p = 0.3\ Nm/rad$ and $k_d = 0.3\ Nms/rad$. The thruster forces applied to the robot at $t_1 = 1\ s$ for a time interval $\Delta t = 0.5\ s$, were $\Sigma F_x = 0.052\ N$ and $\Sigma F_y = -0.595\ N$. The linear Y-velocity of point S is obtained by the slope of the linear Y-translation of the same point, see Fig. 9. Based on it, this velocity was $(\dot{r}_{s\,|\,t_1})_y = 0.0024\ m/s$ at $t_1 = 1\ s$ and $(\dot{r}_{s\,|\,t_2})_y = -0.0195\ m/s$ at $t_2 = 1.5\ s$. Thus, using Eq. (40), *Cepheus*′ total mass is identified as $M^* = 13.56\ kg$.

To verify this result, the robot was weighted before and after the experiment yielding a mean value $M = 13.55\ kg$; this corresponds to an identification relative error equal to 0.1 %.

5.6. Method experimental validation

To validate the experimental results and the developed method, we compare the response of the simulated SRE using the identified parameters, with the experimental response of the actual SRE, obtained during a new experiment, in which, the manipulator joints follow trajectories randomly selected

$$\begin{aligned} q_{d1}(t) &= 0.86 \sin(2\pi t/t_f)\ [rad] \\ q_{d2}(t) &= \sin(2\pi t/t_f)\ [rad] \end{aligned} \tag{47}$$

where q_{d1}, q_{d2} are the desired joint angles for the first and second joint. The trajectory duration is $t_f = 18\ s$.

Fig. 10 shows the time histories of the measured joint angles and rates. The measured SC angle and angular velocity are shown in Fig. 11, and the SC absolute X and Y positions and velocities are shown in Figs. 12 and 13, respectively.

In particular, the second plot of Fig. 11 shows the time histories of the experimentally obtained SC angular velocity together with the predicted one, as obtained by simulating the model with the identified parameters $\boldsymbol{\pi}$ of Table 6 and based on Eq. (43), while the arm joints perform the joint trajectories of the validation experiment. As shown in this plot, given the identified parameters, the SC angular velocity of the robot is predicted accurately.

Similarly, Fig. 13 shows the time histories of the experimentally obtained SC linear velocities in X- and Y- axis together with the predicted ones, obtained by simulating the model with the identified parameters $\boldsymbol{\varphi}$ of Table 6 and based on the kinematic equation (44). Note that the periodic variations of the position and velocity of the tracked point S are due to the rotation of the robot. As shown in this plot, given the identified parameters, the SC linear velocity of the robot is predicted accurately.

Consequently, and as shown in all plots, given the identified parameters, the free-flying dynamics of the robot are predicted accurately, validating the identified parameters and the effectiveness of the developed method.

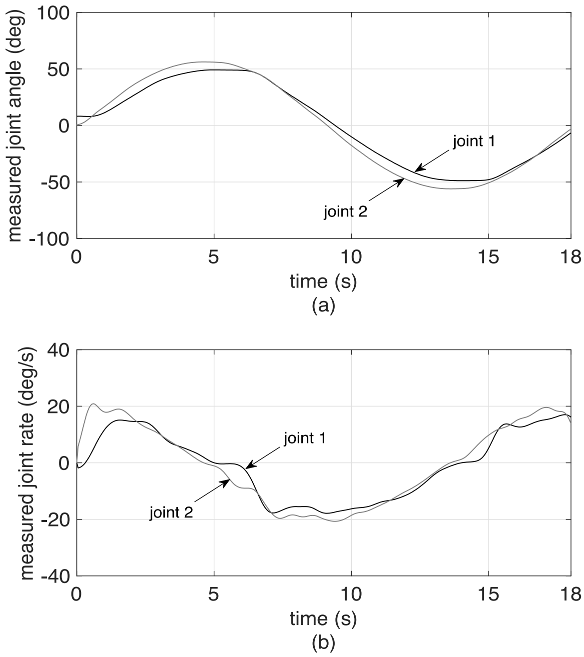

Fig. 10. Measured histories. (a) manipulator joint angles and (b) their rates.

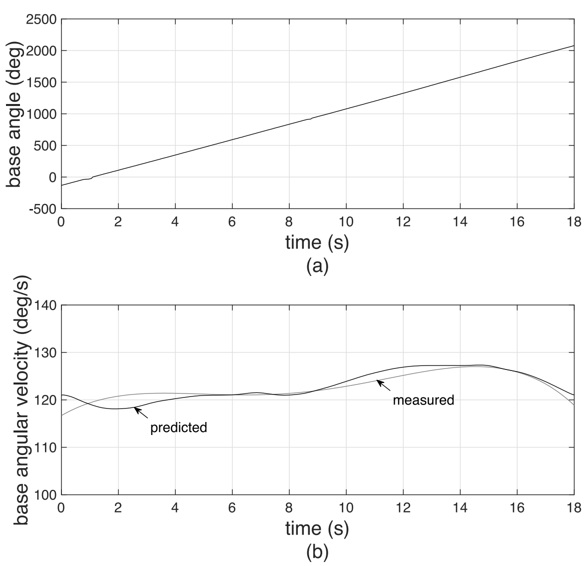

Fig. 11. Measured responses for validation. (a) SC angle and (b) measured and predicted SC angular velocity.

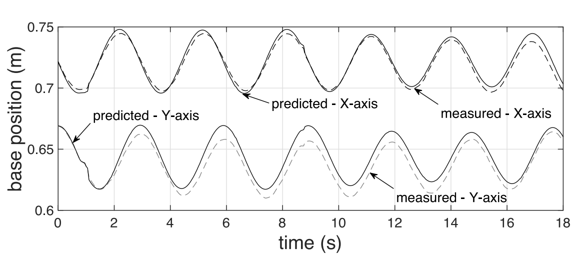

Fig. 12. Measured and predicted SC absolute X and Y position.

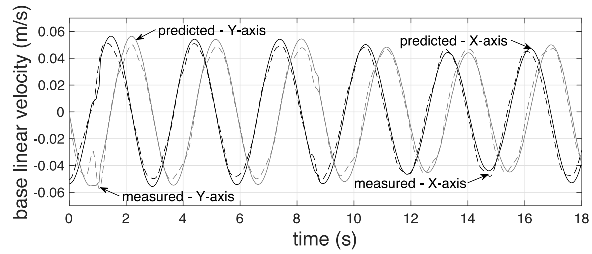

Fig. 13. Measured and predicted SC absolute X and Y velocity.

6. Conclusion

In this paper, a novel parameter identification method is proposed, which identifies all parameters required for the reconstruction of the free-flying space manipulator dynamics. In contrast to other methods, its key advantage is that it does not use acceleration measurements of any variable; thus, it is less sensitive to sensor noise. In addition, it is applicable to multi-arm systems. The identification method is based on the conservation of angular momentum and on system kinematics. To apply the developed method, all manipulator joints are commanded to follow optimized exciting trajectories, while the system is in free-floating mode. Use of the method makes the fully identified free-flying space manipulator dynamics available to model-based control and other advanced control schemes. The method is validated by simulation in the presence of noise and experimentally, with excellent results.

Declaration of competing interest

The authors declare that they have no known competing financial interests or personal relationships that could have appeared to influence the work reported in this paper.

Data availability

No data was used for the research described in the article.

Appendix

The Jacobian matrix $\mathbf{J}_{0,p}$ is given by

$$\mathbf{J}_{0,p} = \begin{bmatrix} \mathbf{1}_{3\times3} & \mathbf{J}_1^{(0)} & \mathbf{J}_2^{(0)} & \mathbf{0}_{3\times N_{rw}} \\ \mathbf{0}_{3\times3} & \mathbf{1}_{3\times3} & \mathbf{0}_{3\times K} & \mathbf{0}_{3\times N_{rw}} \end{bmatrix}_{6\times(6+K+N_{rw})} \tag{A.1}$$

where submatrices $\mathbf{J}_1^{(0)}$ and $\mathbf{J}_2^{(0)}$ are given in [26].

The Jacobian matrix $\mathbf{J}_{i,p}^{(m)}$ is given by

$$\mathbf{J}_{i,p}^{(m)} = \begin{bmatrix} \mathbf{1}_{3\times3} & \mathbf{J}_1^{(m)} & \mathbf{J}_2^{(m)} & \mathbf{0}_{3\times N_{rw}} \\ \mathbf{0}_{3\times3} & \mathbf{1}_{3\times3} & \mathbf{J}_3^{(m)} & \mathbf{0}_{3\times N_{rw}} \end{bmatrix}_{6\times(6+K+N_{rw})} \tag{A.2}$$

where

$$\mathbf{J}_1^{(m)} = -\left[\tilde{\mathbf{r}}_0^{(m)} + \sum_{\substack{j=1\\ j\neq m}}^{n}\sum_{k=1}^{N_j}\tilde{\mathbf{l}}_k^{(j)} + \sum_{k=1}^{N_m}\tilde{\mathbf{v}}_{ki,p}^{(m)} + \sum_{\substack{j=1\\ j\neq m}}^{n}\tilde{\mathbf{e}}_0^{(j)}\right]^{\times} \tag{A.3}$$

and the Jacobian submatrices $\mathbf{J}_2^{(m)}, \mathbf{J}_3^{(m)}$ are given in [26]. The body-fixed barycentric vectors $\tilde{\mathbf{r}}_0^{(m)}$, $\tilde{\mathbf{l}}_k^{(m)}$, $\tilde{\mathbf{v}}_{ki,p}^{(m)}$ and $\tilde{\mathbf{e}}_0^{(m)}$ in (A.3) are given in [26].

The minimum possible set of parameters $\boldsymbol{\pi}$ for a planar two DoF manipulator system is eight parameters, given as

$$\begin{aligned}
\pi_1 &= m_0{}^0r_{0_x}\left(\left(m_1+m_2\right)l_1+m_2r_1\right)/M \\
\pi_2 &= m_0{}^0r_{0_x}m_2l_2/M \\
\pi_3 &= m_0{}^0r_{0_y}\left(\left(m_1+m_2\right)l_1+m_2r_1\right)/M \\
\pi_4 &= m_0{}^0r_{0_y}m_2l_2/M \\
\pi_5 &= {}^0I_0+m_0\left(m_1+m_2\right)\left({}^0r_{0_x}^2+{}^0r_{0_y}^2\right)/M \\
\pi_6 &= \left(m_2l_2\right)\left(m_0l_1+\left(m_0+m_1\right)r_1\right)/M \\
\pi_7 &= {}^1I_1+\left(m_0\left(m_1+m_2\right)l_1^2+2m_0m_2l_1r_1+m_2\left(m_0+m_1\right)r_1^2\right)/M \\
\pi_8 &= {}^2I_2+m_2\left(m_0+m_1\right)l_2^2/M
\end{aligned} \tag{A.4}$$

where m_0,m_1, m_2 are the masses of bodies 0, 1, 2 respectively, ${}^0I_0$, ${}^1I_1$, ${}^2I_2$ are the polar moments of inertia about axes passing from the CM of bodies 0,1,2 respectively. The link parameters ${}^0r_{0_x}$, ${}^0r_{0_y}$, l_1, r_1, l_2 are defined according to the Denavitt Hartenberg convention, and are given as

$$\mathbf{{}^0r_0}=\begin{bmatrix}{}^0r_{0_x} & {}^0r_{0_y} & 0\end{bmatrix}^{\mathrm{T}},\ \mathbf{{}^il_i}=\begin{bmatrix}-l_i & 0 & 0\end{bmatrix}^{\mathrm{T}},\ \mathbf{{}^ir_i}=\begin{bmatrix}r_i & 0 & 0\end{bmatrix}^{\mathrm{T}} \tag{A.5}$$

The minimum set of $\boldsymbol{\varphi}$ parameters for a spatial three DoF manipulator system includes five parameters

$$\begin{aligned}
\phi_1 &= m_0{}^0r_{0_x}/M \\
\phi_2 &= m_0{}^0r_{0_y}/M \\
\phi_3 &= m_3l_3/M \\
\phi_4 &= \left(\left(m_2+m_3\right)l_2+m_3r_2\right)/M \\
\phi_5 &= \left(m_0{}^0r_{0_z}-\left(m_1+m_2+m_3\right)l_1+\left(m_2+m_3\right)r_1\right)/M
\end{aligned} \tag{A.6}$$

The minimum set of $\boldsymbol{\varphi}$ parameters for a planar two DoF manipulator system includes four parameters

$$\begin{aligned}
\phi_1 &= m_0{}^0r_{0_x}/M & \phi_2 &= m_0{}^0r_{0_y}/M \\
\phi_3 &=_1 \left(\left(m_1+m_2\right)l_1+m_2r\right)/M & \phi_4 &= m_2l_2/M
\end{aligned} \tag{A.7}$$

References

[1] A. Flores-Abad, O. Ma, K. Pham, S. Ulrich, A review of space robotics technologies for on-orbit servicing, Prog. Aerosp. Sci. 68 (2014) 1–26.

[2] M. Oda, Space robot experiments on NASDA's ETS-VII satellite-preliminary overview of the experiment results, in: Proc. IEEE Int. Conf. Robot. Autom, Detroit, Michigan, USA, 1999, pp. 1390–1395.

[3] A. Ogilvie, J. Allport, M. Hannah, J. Lymer, Autonomous satellite servicing using the Orbital Express Demonstration Manipulator System, in: Proc. ISAIRAS Hollywood, USA, 2008.

[4] S. Dubowsky, E. Papadopoulos, The kinematics, dynamics, and control of free-flying and free-floating space robotic systems, IEEE Trans. Robot. Autom. 9 (5) (1993) 531–543.

[5] S. Ali Moosavian, E. Papadopoulos, Free-flying robots in space: an overview of dynamics modeling, planning and control, Robotica 25 (5) (2007) 537–547.

[6] R. Bernard, S. L, Albright, Robot Calibration, Chapman & Hall, London, 1993.

[7] J.L. Schwartz, C.D. Hall, System identification of a spherical air-bearing spacecraft simulator, in: Proc 16^{Th} AAS/AIAA Space Flight Mech. Conf, Hawaii, Maui, 2004.

[8] Y. Murotsu, K. Senda, M. Ozaki, S. Tsujio, Parameter identification of unknown object handled by free-flying space robot, AIAA J. Guid. Control, Dyn. 17 (3) (1994) 488–494.

[9] R. Lampariello, G. Hirzinger, Modeling and experimental design for the on-orbit inertial parameter identification of free-flying space robots, in: Proc. IDETC/CIE 2005 ASME 2005 Int. Des. Eng. Tech. Conf. Comp. Inf. Eng. Conf, Long Beach, CA, USA, 2005, pp. 1–10.

[10] W. Rackl, R. Lampariello, A. Albu-Schaffer, Parameter identification methods for free-floating space robots with direct torque sensing, IFAC Proc. 46 (19) (2013) 464–469.

[11] S.-Y. Nabavi-Chashmi, S.-M.B. Malaek, Inertial parameter identification using contact force information for an unknown object captured by a space manipulator, Acta Astronaut. 131 (2017) 69–82.

[12] M. Ekal, R. Ventura, On inertial parameter estimation of a free-flying robot grasping an unknown object, in: Proc 5^{Th} Int. Conf. Con.Dec. Inf. Tech, Thessaloniki, Greece, 2018, pp. 815–821.

[13] W. Xu, Z. Hu, Y. Zhang, Z, B. Liang, On-orbit identifying the inertia parameters of space robotic systems using simple equivalent dynamics, Acta Astron. 132 (2017) 131–142.

[14] K. Yoshida, S. Abiko, Inertia parameter identification for a free-flying space robot, in: AIAA Guidance, Navigation, and Control Conference, Monterey, CA, 2002.

[15] O. Ma, H. Dang, On-orbit identification of inertia properties of spacecraft using a robotic arm, AIAA J. Guid. Control, Dyn. 31 (6) (2008) 1761–1771.

[16] T.-C. Nguyen-Huynh, I. Sharf, Adaptive reactionless motion and parameter identification in post-capture of space debris, AIAA J. Guid. Control, Dyn. 36 (2) (2013) 404–414.

[17] L. Zong, J. Luo, M. Wang, J. Yuan, Parameters concurrent learning and reactionless control in post-capture of unknown targets by space manipulators, Nonlinear Dynam. 96 (1) (2019) 443–457.

[18] M. Ekal, R. Ventura, On the accuracy of inertial parameter estimation of a free-flying robot while grasping an object, J. Intell. Robot. Syst. 98 (1) (2020) 153–163.

[19] B. Naveen, S.V. Shah, A.K. Misra, Momentum model-based minimal parameter identification of a space robot, AIAA J. Guid. Control, Dyn. 42 (3) (2018) 508–523.

[20] E. Papadopoulos, F. Aghili, O. Ma, R. Lampariello, Robotic manipulation and capture in space: A survey, Front. Robot. AI (2021).

[21] O.-O. Christidi-Loumpasefski, K. Nanos, E. Papadopoulos, On parameter estimation of space manipulator systems using the angular momentum conservation, in: Proc. IEEE Int. Conf. Robot. Autom, Singapore, 2017, pp. 5453–5458.

[22] O.-O. Christidi-Loumpasefski, G. Rekleitis, E. Papadopoulos, Concurrent parameter identification and control for free-floating robotic systems during on-orbit servicing, in: Proc. IEEE Int. Conf. Robot. Autom, Paris, France, 2020.

[23] E. Papadopoulos, On the Dynamics and Control of Space Manipulators (Ph.D. dissertation), Dept. Mech. Eng. MIT, Cambridge, MA, 1990.

[24] P.C. Hughes, E. Papadopoulos, Spacecraft Attitude Dynamics, in: Series Dover Books on Engineering, Dover Publications, 2004.

[25] S. Ali Moosavian, E. Papadopoulos, Explicit dynamics of space free-flyers with multiple manipulators via SPACEMAPLE, Adv. Robot. 18 (2) (2004) 223–244.

[26] S. Ali Moosavian, E. Papadopoulos, On the kinematics of multiple manipulator space free-flyers and their computation, J. Robot. Syst. 15 (4) (1998) 207–216.

[27] E. Papadopoulos, S. Dubowsky, Coordinated manipulator/space-craft motion control for space robotic systems, in: Proc. IEEE Int. Conf. Robot. Autom, Sacramento, CA, 1991, pp. 1696–1701.

[28] H.F. Grip, T.I. Fossero, T.A. Johansent, A. Saberi, A nonlinear observer for integration of GNSS and IMU measurements with gyro bias estimation, in: Proc. Amer. Contrl. Conf, 2012, pp. 4607–4612.

Olga-Orsalia Christidi-Loumpasefski received her Diploma in Mechanical Engineering with first-class honors from the University of Patras, Greece, in 2015. She is currently pursuing a Ph.D. degree in Mechanical Engineering at the National Technical University of Athens (NTUA).

Her research interests are in the area of space robotics, in-orbit servicing, active space debris removal, dynamics, identification and control of robotic systems on orbit. She is a member of the Technical Chamber of Greece (TEE) and a Member of IEEE and AIAA.

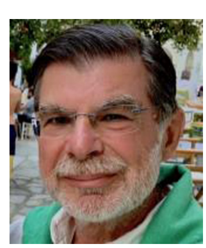

Evangelos Papadopoulos received his Diploma from the National Technical University of Athens (NTUA) in 1981, and his M.S. and Ph.D. degrees from MIT in 1983 and 1991 respectively, all in Mechanical Engineering.

He was a systems analyst with the Hellenic Navy, Athens, Greece, from 1985 to 1987. In 1991 he joined McGill U. and the Centre for Intelligent Machines (CIM) as an Assistant Professor. Currently, he is a Professor with the Department of Mechanical Engineering at the NTUA, where he teaches courses in the areas of Robotics, Systems, Controls, and Mechatronics. His research interests are in robotics, modeling and control of dynamic systems, mechatronics, and design. He serves as an Associate Editor for the *Machine and Mechanism Theory*, and the *Frontiers in Space Robotics*, while previously he has served as an Associate Editor for the *IEEE Transactions on Robotics*, the *ASME J. of Dynamic Systems, Measurement and Control*, the *IEEE Robotics and Automation Letters (RAL)*, the *IEEE Robotics and Automation Society (RAS) Conference Editorial Board*, (Mechanics, Design and Control), and as a Guest Editor for the *IEEE/ASME Transactions on Mechatronics*. He has published more than 300 technical articles in journals and refereed conference proceedings. He is a Life Fellow of the IEEE, a Fellow of the ASME, an Associate Fellow of the AIAA, a Member of the IFToMM, and of the Technical Chamber of Greece. He is an elected member of the Sigma Xi.